Three-dimensional water impact at normal incidence to a blunt structure

I. K. Chatjigeorgiou[1,2], M. J. Cooker[1], A. A. Korobkin[1]

[1]School of Mathematics, University of East Anglia, Norwich, NR4 7TJ, UK
[2]School of Naval Architecture and Marine Engineering, National Technical University of Athens,

15773 Greece

Abstract

The three-dimensional (3D) water impact onto a blunt structure with a spreading rectangular contact region is studied. The structure is mounted on a flat rigid plane with the impermeable curved surface of the structure perpendicular to the plane. Before impact, the water region is a rectangular domain of finite thickness bounded from below by the rigid plane and above by the flat free surface. The front free surface of the water region is vertical, representing the front of an advancing steep wave. The water region is initially advancing towards the structure at a constant uniform speed. We are concerned with the slamming loads acting on the surface of the structure during the initial stage of water impact. Air, gravity and surface tension are neglected. The problem is analysed by using some ideas of pressure-impulse theory, but including the time-dependence of the wetted area of the structure. The flow caused by the impact is 3D and incompressible. The distribution of the pressure-impulse (the time-integral of pressure) over the surface of the structure is analysed and compared with the distributions provided by strip theories. The total impulse exerted on the structure during the impact stage is evaluated and compared with numerical and experimental predictions. An example calculation is presented of water impact onto a vertical rigid cylinder. Three-dimensional effects on the slamming loads are of main concern in this study.

Key words: Free-surface flows, slamming loads, three-dimensional effects

1. Introduction

The present analysis deals with the 3D effects on water impact loads. Such loads are of concern for offshore structures subjected to steep and breaking wave impact [1], tsunami bore forces on coastal structures [2-3], interaction of dry-bed surges and broken waves with buildings [4-5]. Interaction of

jets with obstacles is of concern in problems of violent sloshing in liquefied natural gas tanks of NO-96 type [6]. The inner surface of these tanks is manufactured with tongues of length about 3 cm perpendicular to the main flat surface. Impacts of sloshing waves and jets on these tongues may damage the inner structure of the tank. The loads exerted on structures by such water impacts are much higher than any loads associated with propagating gravity waves, but they have short duration. The geometrical configurations of these impact problems are complicated to analyse. The studies of the loads have been performed numerically by Computational Fluid Dynamics (CFD) and Smoothed Particle Hydrodynamics (SPH) methods [7-8], or by laboratory experiments [3].

Theoretical studies (see [1] for review) assume simplified profiles of the wave front, either vertical, parallel to the surface of the structure, or slightly inclined. In the theoretical models, the flow caused by the impact is assumed to be potential, with viscous, gravity and surface tension effects neglected. It has been shown [1] that the shape of the free surface of an impacting liquid and the shape of the rigid boundaries far from the place of impact provide negligible contributions to the loads. This makes it possible to consider simplified impact configurations using the geometry near the site of impact with flat boundaries in many situations of practical importance. The simplest model relies on the concept of pressure-impulse [1, 9]. In this model, the time dependence of the size of the wetted area of the structure's surface is not included. It is assumed that the structure is wetted instantly. Only the velocity of the impact and the shape of the impact region are important. This model is well validated against numerical and experimental results [1]. The model has been applied to practical problems in two-dimensional (2D) and 3D formulations. However, the finite length of the structure was not included. The finite duration of the impact was taken into account by Korobkin [10] within the 2D Wagner model, where the size of the wetted part of the wall was calculated as part of the solution.

Impacts on a structure by steep, breaking and broken waves are [the most] dangerous types of impact. Such waves may entrain significant amounts of air before the impact. The water in the impact region should be modelled as an aerated fluid [11]. However, the pressure impulse has been shown to be independent of the air fraction in water [12]. It has also been shown that the maximum stresses in an elastic wall impacted by a breaking wave are also independent of the air fraction in the impact region [13]. Truly 3D-dimensional problems of water impact are still complicated to study, even within pressure-impulse theory.

Three-dimensional unsteady flow of water impact, in which the impact region is expanding in time, have been solved only for lower half-spaces, with circular and elliptic contact regions on the flat boundary of the flow region, of infinite extent [14-15]. The added mass of a rectangular plate descending suddenly into a flat free surface was computed by Meyerhoff [16]. Three-dimensional impact problems are complicated due to the mixed type of the governing boundary value problems. Mixed boundary value problems require Neumann and Dirichlet conditions to be satisfied on different portions of the boundary. Analytical studies conducted in 3D exist only for special cases of violent impact, i.e. water entry problems [14-15] and for ideal geometries such as elliptic paraboloids [17]. The major problem comes from an additional unknown, which is the time-dependent contact region – the zone in which the liquid is in contact with the structure. It is in the contact region, where a Neumann boundary condition is imposed and outside it a Dirichlet condition. The solutions of mixed boundary value problems are singular at the contact line – the curve which separates the parts of the boundary with different types of boundary condition.

The most realistic model of wave impact is that which considers plunging overturning breaking waves for which the current knowledge relies mainly on experiments [18-19]. This model includes too many parameters, making it not very practical from the point of view of load predictions. The essential parameters are the wave height, water depth and the speed of impact [1]. These parameters lead to a simplified approach known as *steep wave impact*, which assumes a vertical liquid front face at the time of the impact with the structure. Under these conditions we expect the greatest hydrodynamic loads. In the present study it is suggested to exclude the water depth between the approaching wave and the structure from the model and consider a semi-infinite rectangular liquid region approaching the structure at a constant speed. That is, as a wave approaches the structure the wave trough descends exposing the face of the structure, and the forward face of the wave steepens to become parallel to the structure's vertical front. Then the structure surface is dry just before impact. Such a situation was observed in laboratory experiments by Mogridge and Jameison [20]. We assume that the assumption of zero water depth in front of the structure provides useful estimates of the maximum loads.

The most realistic situation that is included in the concept of steep wave impact is the *dam-break flow*, namely a volume of liquid originally at rest and confined by a vertical barrier which is suddenly removed, releasing the liquid. Theoretical studies on dam-break flows are usually performed in 2D, without taking into account the presence of a structure in the path of the flow [21-

27]. Three-dimensional studies of dam-break flows, known also as dry-bed surges, rely on numerical methods. Abdolmaleki et al. [28] simulated the impact on a vertical wall resulting from a dam-break flow. A dam-break flow and its impact on a rectangular obstacle were studied also by Aurelli et al. [29]. Both studies were conducted using the Navier-Stokes solver FLUENT. Their common characteristic was that, when the flow met the structure, the flow was too shallow for impact. Yang et al. [30] used a 3D numerical model based on the unsteady Reynolds equations to simulate near-field dam-break flows and estimate the impact forces on obstacles. Kleefsman et al. [7] applied a Volume-of-Fluid (VOF) method to simulate the impact of a dam-break flow on rectangular bodies. The cases considered in [7] resemble flood-like flows and they cannot be characterized as violent wave impacts. Ramsden [4] concluded that the dry-bed surges do not lead to impact forces in experiments. However, such forces of large magnitude and short duration were computed by Cummins et al. [8]. To the authors' best knowledge there have been no 3D studies, even using numerical methods, for complicated convex geometries, such as circular cylinders.

The main idea of the present study is to consider the most dangerous scenario of 3D water impact, when the bottom around the structure is dry, or becomes dry before the impact (see Mogridge and Jamieson [20]), and a liquid mass of finite depth (and infinite extent in the horizontal directions) approaches the structure with a vertical front face moving at a constant speed (see figure 1). The outlined condition is idealized and the prediction of the impact loads should be carefully compared with the loads experienced by the structure in realistic conditions.

We will determine the impact loads acting on the vertical rigid plate and compare them with those provided by 2D strip theories. The loads predicted by the strip theories are expected to approximate well the 3D loads in two limiting cases: when the plate width is much larger or much smaller than the water depth. The present formulation approximates the 3D impact on a vertical column of rectangular section, which has been previously studied by CFD and SPH methods. The method of this paper allows us to derive closed-form relations for the pressure-impulse and the total impulse exerted on the plate. The present study models the impact conditions in terms of the aspect ratio of the wetted part of the structure, and makes clear the conditions in which the 2D strip theories provide reasonable approximations of the loads.

The method is applied to the time-dependent problem of water impact onto a circular cylinder, where the vertical front of the water region initially just touches the cylinder. Then the wetted area

of the cylinder surface expands in time, finally wetting half of the cylinder. The boundary of the contact region is approximated by straight vertical lines, the positions of which are predicted by 2D theories of water impact with (Wagner's approach) and without (von Karman's approach) account for the deformation of the vertical free surface due to the impact. The forces exerted on the cylinder are evaluated within the 3D impact theory. The difference between the forces predicted by the strip theories and the forces from the 3D model was found to be significant.

The study is structured as follows: in Section 2 we formulate the 3D impact problem and its 2D approximations; the 3D solution of that problem is derived in Section 3, while relevant numerical results and comparisons with 2D strip theory approximations are provided in Section 4; Section 5 is dedicated to the calculation of the total impulse exerted on the structure due to the impulsive pressure. The solution method is extended in Section 6 to tackle the 3D time-dependent impact problem for a circular cylinder. Time-varying hydrodynamic loads exerted on the circular cylinder are calculated. In Section 7, the results predicted by the developed method are compared with reported numerical and experimental data. The conclusions are drawn in Section 8 and the supplementary material of the study is provided in Appendix A.

2. The hydrodynamic boundary value problem and its 2D versions

The interaction between a liquid volume of thickness H and a vertical rigid plate of width $2L$ is considered in the Cartesian coordinate system x, y, z with the origin at the centre of the plate at the water level (see figure 1). The liquid volume moves towards the plate at a uniform speed V. The liquid occupies the semi-infinite region $x > 0, -H < z < 0$ at the time of impact, $t = 0$, the time when the forward front face of the wave has met the plate. The plane $z = -H$ is the rigid bottom and the plane $z = 0$ is the horizontal free surface of the liquid before impact. The vertical boundary of the liquid region, $x = 0$, consists of the contact region, $|y| < L$, between the liquid and the rigid plate, and the liquid free surface, where $|y| > L$. The liquid is assumed to be inviscid and incompressible. Gravity and surface tension effects are neglected. During the initial stage of impact the displacements of the liquid particles are small. This makes it possible to linearize the boundary conditions and impose them on the initial position of the liquid boundary. This approximation is known as pressure-impulse theory [9]. The formulated problem is linear with mixed boundary conditions on the vertical boundary of the flow region. The velocity of the flow caused by impact is described by a velocity potential which changes from ϕ_b before impact to ϕ_a after impact [9]. The

pressure-impulse is a function of x, y, z, which is defined to be the time-integral of the pressure over the short time interval $[0, \Delta t]$ of impact.

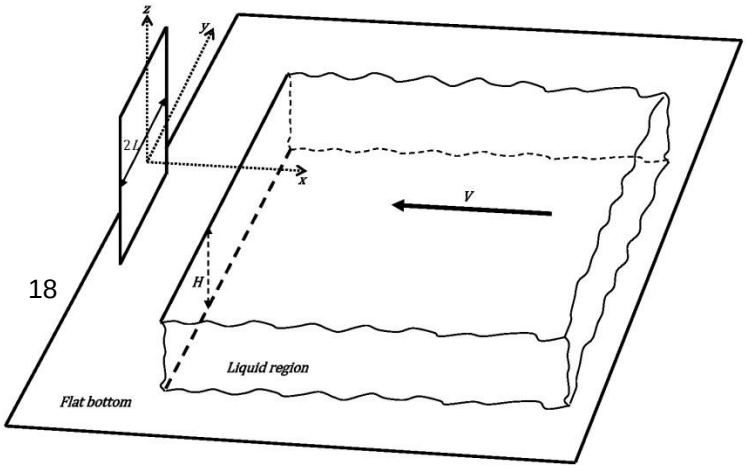

Figure 1. Configuration of the water impact problem with a vertical plate.

For small duration of the impact stage, Δt, the pressure-impulse is defined by

$$P(x,y,z) = -\rho[\phi_b(x,y,z) - \phi_a(x,y,z)] \tag{2.1}$$

where ρ is the water density. For a uniform flow of speed V before impact, $\phi_b = -Vx$ and $\phi_a \sim -Vx$ as $x \to \infty$. In Section 6 we will consider L to increase with time but for now we treat the instantaneous flow.

The problem is treated in non-dimensional (tilde) variables, $x = L\tilde{x}$ $y = L\tilde{y}$ $z = L\tilde{z}$, $\phi = VL\tilde{\phi}$ $p = -\rho VL\phi/\Delta t$. The tildes are dropped below. The scaled boundary value problem for the non-dimensional pressure impulse, $\phi(x,y,z)$, has the form

$$\phi_{xx} + \phi_{yy} + \phi_{zz} = 0, \qquad (x > 0, -\infty < y < \infty, -h < z < 0), \tag{2.2}$$

$$\phi = 0, \quad (x > 0, -\infty < y < \infty, z = 0) \text{ and } (x = 0, |y| > 1, -h < z < 0), \tag{2.3}$$

$$\phi_z = 0, \qquad (x > 0, -\infty < y < \infty, z = -h), \tag{2.4}$$

$$\phi_x = 1, \qquad (x = 0, |y| < 1, -h < z < 0), \tag{2.5}$$

$$\phi \to 0, \quad (x^2+y^2\to\infty). \tag{2.6}$$

The model equations (2.2)-(2.6) contain only one parameter $h = H/L$, which is the aspect ratio of the rectangular plate. Condition (2.3) follows from the linearized dynamic condition on the liquid free-surface and the initial condition that the potential ϕ of the flow induced by the impact is zero before the impact. Condition (2.5) on the plate, accounts for the fact that the liquid hits the plate with a non-zero normal velocity component, but subsequently cannot penetrate the plate, and stays in sliding contact with the plate. The top and the side views of the plate at the instant of impact are shown in the sketch of figure A.1 of the supplementary material.

For a narrow plate, $h \gg 1$, the potential is approximately independent of the vertical coordinate z far from the upper free-surface. Correspondingly, for a very wide plate, $h \ll 1$, the potential is independent of the transverse coordinate y far from the edges of the plate. These approximations correspond to the strip theory solutions, $\phi^{(h)}(x,y)$ and $\phi^{(v)}(x,z)$, where the superscripts (h) and (v) indicate that the strips are respectively horizontal and vertical. According to strip theory, the 3D plate is discretized vertically or horizontally by narrow strips perpendicular to the much longer dimension of the plate. Thus, the z- or the y-variation of the potential can be omitted and the problem is reduced to 2D. The potential $\phi^{(h)}(x, y)$ on the plate, within the strip theory approximation, is given by [16, 31]

$$\phi^{(h)}(0,y) = -\sqrt{1-\overline{y^2},\ |y|} < 1,\ h \gg 1. \tag{2.7}$$

This approximation is not valid near the upper free-surface, $z = 0$, where the potential should approach zero as specified by condition (2.3). The following vertical strips approximation of the potential, $\phi^{(v)}(x,z)$, on the plate, $x = 0, -h < z < 0$, has been given in references [9] and [32]; it is:

$$\phi^{(v)}(0,z) = \frac{8h}{\pi^2}\sum_{n=1}^{\infty}\frac{\sin[(2n-1)\pi z/(2h)]}{(2n-1)^2} \quad h \ll 1. \tag{2.8}$$

The velocity potential (2.8) is not valid near the edges of the plate, $y = \pm 1$.

We shall obtain the solution of the 3D problem (2.2)-(2.6) using series comprising trigonometric and Mathieu functions. Afterwards we will compare the potential $\phi(0,y,z)$ on the vertical plate with approximations (2.7) and (2.8) in order to find the ranges of the parameter h, in which these approximations can be used. In Section 6 we will use these results to solve the problem of water impact on a vertical circular cylinder, in which the half-width L of the wetted region increases with time in a way that depends on the shape and curvature of the body being hit by the water front.

3. Solution of the 3D problem of wave impact

The solution of the problem (2.2)-(2.6) is sought in the form

$$\phi(x,y,z) = -\frac{2}{h}\sum_{n=1}^{\infty} \lambda_n^{-1}\phi_n(x,y)\sin(\lambda_n z), \qquad \lambda_n = \frac{\pi}{2h}(2n-1), \tag{3.1}$$

where the coefficients $\phi_n(x,y)$ satisfy the following mixed boundary-value problem of modified Helmholtz type, in which subscripts x and y denote partial derivatives:

$$\phi_{nx} + \phi_{ny} - \lambda_n^2 \phi_n = 0, \ (x > 0), \tag{3.2}$$

$$\phi_n = 0, \ (x = 0, |y| > 1), \tag{3.3}$$

$$\phi_{n,x} = 1, \ (x = 0, |y| < 1), \tag{3.4}$$

$$\phi_n \to 0, \ (x^2 + y^2 \to \infty). \tag{3.5}$$

The problem (3.2)-(3.5) was considered by Egorov [33], who investigated a rigid plate impact onto the free-surface of a weakly compressible liquid.

To find the solution of (3.2)-(3.5) we consider the interval $x = 0, -1 < y < 1$, as a degenerate ellipse with semi-axes a and b, where $a \to 1$ and $b \to 0$. A sketch of the plate represented by a degenerate elliptical cylinder is shown in figure A.2 of the supplementary material.

We use 2D elliptical coordinates (u, v), defined by $x = c\sinh u \sin v$ and $y = c\cosh u \cos v$ where $c = \sqrt{a^2 - b^2}$ is the half distance between the foci. The fluid occupies the region $u_0 < u, 0 \le v \le \pi$

where $u = u_0$ is the surface of the elliptical plate. For a plate of zero thickness we consider the limit as $a \to 1, b \to 0, c \to 1$ and $u_0 \to 0$. Equation (3.2) has the following form:

$$\frac{1}{\cosh 2u - \cos 2v}\left(\frac{\partial^2 \phi_n}{\partial u^2} + \frac{\partial^2 \phi_n}{\partial v^2}\right) + 2\left(\frac{\lambda_n}{2}\right)^2 \phi_n = 0. \tag{3.6}$$

Using separation of variables $\phi_n(u,v) = U_n(u)V_n(v)$, equation (3.6) provides two differential equations for $U_n(u)$ and $V_n(v)$:

$$\frac{d^2 U_n(u)}{du^2} - (\sigma - 2\mu_n \cosh 2u)U_n(u) = 0, \ (0 \le u), \tag{3.7}$$

$$\frac{d^2 V_n(v)}{dv^2} + (\sigma - 2\mu_n \cos 2v)V_n(v) = 0, \ (0 \le v \le \pi), \tag{3.8}$$

where $\mu_n = -(\lambda_n/2)^2$ and σ are the separation constants of the Mathieu equations. The former is known as the Mathieu parameter. The boundary condition (3.3) provides $\phi_n(u,0) = \phi_n(u,\pi) = 0$ and yields the boundary conditions for equation (3.8), $V_n(0) = V_n(\pi) = 0$. Non-trivial solutions of the periodic Mathieu equation (3.8) with zero boundary conditions exist only for certain values of σ known as the characteristic values of (3.8) [34]. These non-trivial solutions are known as the odd periodic Mathieu functions $se_{2m+1}(v, -q_n)$, where $q_n = -\mu_n$ and m is a non-negative integer. The corresponding characteristic values are denoted by $\sigma_n^{(m)}$. The solution of the radial (or modified) Mathieu equation (3.7) with these values of σ, and decaying as $u \to \infty$, are known as the odd radial Mathieu functions of the third kind $Ms^{(3)}_{2m+1}(u, -q_n)$. Then the products $\varphi_n^{(2m+1)}(u,v) = Ms^{(3)}_{2m+1}(u, -q_n)se_{2m+1}(v, -q_n)$ satisfy Helmholtz's equation (3.2) and conditions (3.3) and (3.5).

The boundary condition (3.4) is now

$$\phi_u = \sin v, \ (u = 0, \ 0 \le v \le \pi), \tag{3.9}$$

where subscript u denotes partial derivative. To satisfy (3.9), we write

$$\phi_n(u,v) = \sum_{m=0}^{\infty} D^{(n)}_{2m+1} \varphi_n^{(2m+1)}(u,v), \tag{3.10}$$

where the coefficients $D^{(n)}_{2m+1}$ are to be determined. The body boundary condition (3.9) yields

$$\sum_{m=0}^{\infty} D^{(n)}_{2m+1} Ms^{(3)}_{2m+1}(0,-q_n)\, se_{2m+1}(v,-q_n) = \sin v, \quad (0 \le v \le \pi), \tag{3.11}$$

where the prime is the u-derivative. Multiplying (3.11) by $se_{2k+1}(v,-q_n)$, integrating from $v=0$ to $v=\pi$, and using the orthogonality relation of the periodic Mathieu functions ([34]; 20.5.3), we arrive at the following formula for the expansion coefficients $D^{(n)}_{2m+1}$:

$$D^{(n)}_{2m+1} = \frac{1}{\frac{\pi}{2} Ms'^{(3)}_{2m+1}(0,-q_n)} \int_0^{\pi} se_{2k+1}(v,-q_n)\sin v\, dv. \tag{3.12}$$

Note that the periodic Mathieu functions are orthogonal in both $[0,2\pi]$ and $[0,\pi]$ intervals.

The integral in (3.12) is evaluated using the series expansion ([35], 8.611.3):

$$se_{2k+1}(v,-q_n) = \sum_{r=0}^{\infty} B^{(2k+1)}_{2r+1}(-q_n)\sin[(2r+1)v], \tag{3.13}$$

where the coefficients $B^{(2k+1)}_{2r+1}$ of the odd periodic Mathieu functions depend on $-q_n$. Then

$$D^{(n)}_{2m+1} = \frac{B^{(2k+1)}_{2m+1}(-q_n)}{Ms'^{(3)}_{2m+1}(0,-q_n)}. \tag{3.14}$$

The potentials $\phi_n(u,v)$ are given by

$$\phi_n(u,v) = \sum_{m=0}^{\infty} B^{(2m+1)}_{1}(-q_n) \frac{Ms^{(3)}_{2m+1}(u,-q_n)}{Ms'^{(3)}_{2m+1}(0,-q_n)}\, se_{2m+1}(v,-q_n) \tag{3.15}$$

M_{2n+1}^{s} n

In the following, only the velocity potential on the plate at $u = 0$, where $\cos v = y$, is considered. Equations (3.1) and (3.15) provide the velocity potential on the vertical plate:

$$\phi(0,y,z) = \sum_{m=0}^{\infty}\sum_{n=1}^{\infty} C_{mn}(h)\, ce_{2m+1}(v,-q_n)\sin(\lambda_n z) \tag{3.16}$$

$$C_{mn}(h) = -\frac{4}{(2n-1)\pi}\frac{B_1^{(2m+1)}(-q_n)}{Ms'^{(3)}_{2m+1}(0,-q_n)}, \tag{3.17}$$

where $\cos v = y$ and

$$Ms^{(3)}_{2m+1}(0,-q_n) = \frac{4(-1)^{m+1}}{\pi\lambda_n A^{(2m+1)}(q_n)}\, ce_{2m+1}(0,q_n). \tag{3.18}$$

Equation (3.18) was derived using relations for the radial Mathieu functions with negative Mathieu parameter ([34], 20.8.9 and 20.8.11), the asymptotic forms of the modified Bessel functions of zero argument, and the Wronskian of the modified Bessel functions ([34], 9.6.15). The even periodic Mathieu functions are defined by

$$ce_{2m+1}(v,q_n) = \sum_{r=0}^{\infty} A^{(2m+1)}_{2r+1}(q_n)\cos[(2r+1)v], \tag{3.19}$$

where $A^{(2m+1)}_{2r+1}(q_n)$ denote the expansion coefficients of the even periodic Mathieu functions.

Note that q_n is related to h by $q_n = [\pi(2n-1)/(4h)]^2$. Taking the limits as $h \to \infty$ and $h \to 0$ we exploit the asymptotics of $Ms^{(3)}_{2m+1}(0,-q_n)$ and $Ms'^{(3)}_{2m+1}(0,-q_n)$ as $q_n \to 0$ and $q_n \to \infty$, respectively. Both behaviours are found from asymptotic expansions of the Bessel functions. It can be shown that the velocity potential (3.16)-(3.17) can be reduced to the 2D strip theories (2.7) and (2.8).

4. Numerical results

The double series in (3.16) are truncated, $0 \le m \le M$ and $1 \le n \le N$ and evaluated using purpose-made routines for computing the coefficients $A^{(2m+1)}_{2r+1}(q_n)$ and $B^{(2m+1)}_{1}(-q_n)$ and the Mathieu

functions. In figure A.3 of the supplementary material we present a convergence study for equation (3.16) based on the truncation of the involved infinite series.

Figure 2 shows the vertical distribution of the velocity potential at the vertical section $y = 0.5$, given for different values of h. The associate curves at the vertical section $y = 0$ are shown in figure A.4 of the supplementary material. The potential is symmetric with respect to $y = 0$. The 3D solution tends to the 2D solution (2.7) for $h > 100$. Also, figure 2 shows the velocity potential calculated by the second 2D approximation (2.8), valid for $h \ll 1$. Here only the case $h = 0.5$ is shown. It is seen that (2.8) provides a good approximation of the potential for $h \ll 1$ and far from the plate edges. Near the plate edges, 3D effects are important for any h.

The range of validity of the approximate solution (2.8) is shown in figure 3. This figure corresponds to the horizontal section at $z/h = -0.5$. The associate results for $z/h = -1$ are shown in figure A.5 of the supplementary material. The plots demonstrate that (2.8) can be used for $h < 1/10$ over 80% of the length of the plate but is invalid near the plate edges.

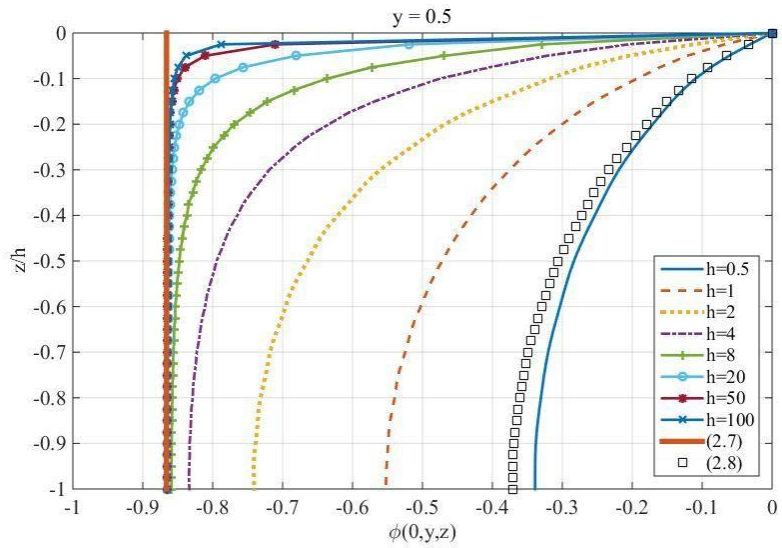

Figure 2. Vertical variation of the velocity potential (3.16) at $x = 0$, $y = 0.5$ for increasing aspect ratio $h = H/L$. The thick solid line depicts the 2D solution (2.7) which is approached by the 3D solution for $h \gg 1$. The square symbols '□' depict the 2D solution (2.8) with $h = 0.5$.

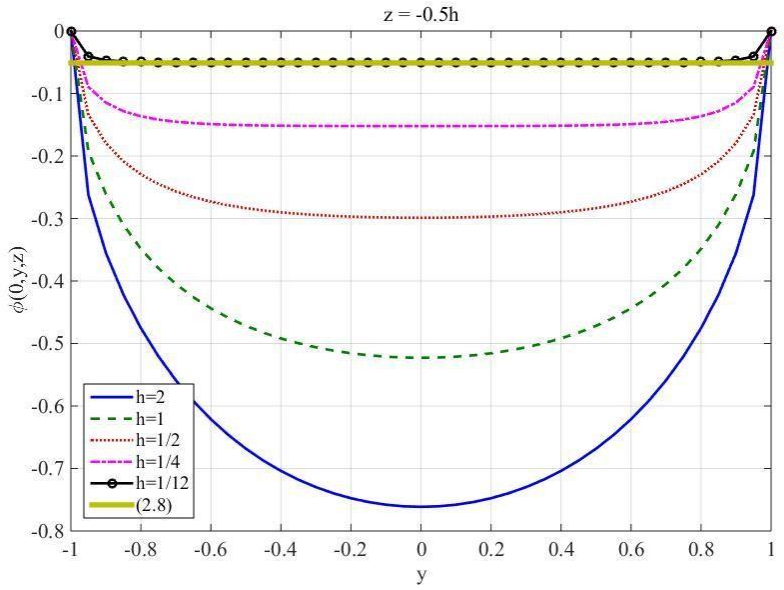

Figure 3. The velocity potential (3.16) at $z/h = -0.5$ for decreasing height to length ratio $h = H/L$. The thick solid line corresponds to the 2D approximation (2.8), which is valid for small h.

5. Total impulse on the plate due to the impulsive pressure

The velocity potential ϕ given by (3.16) is used in this section to evaluate the total impulse acting on the vertical rigid plate due to water impact. We study the dependence of the total impulse on the plate dimensions for different aspect ratios. The total impulse on the plate arises from the integration of the impulsive pressures over the impacted area. Cooker and Peregrine [9] define the pressure-impulse as the time integral of the pressure, over the short time interval of impact. According to Bagnold [36] the pressure-impulse (at a given point) is approximately constant. This is partly confirmed by the measurements of Richert [37] and suggests that the pressure-impulse is a better physical quantity to model than the peak pressure. Cooker and Peregrine [9] define the pressure-impulse as

$$P(x,y,z) = \int_0^{\Delta t} p(x,y,z,t)\,dt, \tag{5.1}$$

where the pressure p is approximated by the time derivative of minus the velocity potential times the water density. In accord with (5.1), the pressure-impulse $P(x,y,z) = -\rho\phi(x,y,z)$, where $\phi(x,y,z)$ is the change in velocity potential brought about by the impact. The total impulse I, is the integral over the contact region of the pressure-impulse. Hence

$$I(h)=-\int_{-h}^{0}\int_{-1}^{1}\phi(0,y,z)\,dy\,dz \tag{5.2}$$

The scale of the total impulse is $\rho V L^3$. The velocity potential on the plate in the 3D problem is given by (3.16) and the 2D solutions for $h \gg 1$ and $h \ll 1$ by (2.7) and (2.8), respectively. Substituting (2.7) and (2.8) successively in (5.2), we obtain the following asymptotic formulae for $I(h)$:

$$I^{(h)}(h)=\frac{\pi}{2}h+O(1),\ \text{as}\ h\to\infty, \tag{5.3}$$

$$I^{(v)}(h)=\frac{28\zeta(3)}{\pi^3}h^2\sim 1.0855h^2+o(h^2),\ \text{as}\ h\to 0, \tag{5.4}$$

where $\zeta(3)=1.202056903$. The superscript (h) in (5.3) indicates that this formula is provided by the horizontal strip theory. The superscript (v) in (5.4) indicates that the vertical strip theory is used.

Substituting the exact formula (3.16) in (5.2) and using the associated negative Mathieu parameter expressions ([34]; 20.8.4 and 20.8.5), we obtain the total impulse as a function of h:

$$I(h)=\frac{4h^2}{\pi^3}\sum_{m=0}^{\infty}\sum_{n=1}^{\infty}\frac{(-1)^m A_{2m+1}^{(2m+1)}(q_n)\,se_{2m+1}(0,q_n)}{(n-\frac{1}{2})^3\,Ms'_{2m+1}(0,-q_n)}. \tag{5.5}$$

Note that the h-dependence of $I(h)$ in (5.5) comes also through the Mathieu parameter q_n. The total impulse (5.5) and the 2D approximations (5.3) and (5.4) are plotted in figure 4 as functions of the aspect ratio h. The range of interest is $0<h<1$. Figure 4 demonstrates that the small-h approximation (5.4) can be used only for $0<h<0.3$. Both approximations, $I^{(h)}(h)$ and $I^{(v)}(h)$, exceed $I(h)$ in $0<h<1$ due to the 3D end-effect near the upper free-surface for $I^{(h)}(h)$ and the end-effect near the vertical edges of the plate for $I^{(v)}(h)$. The graph for $h>1$ is shown in figure A.6 of the supplementary material. We note that $I^{(v)}(h)$ and $I(h)$ differ by a constant value of order $O(1)$ due to the 3D end-effect near the upper free-surface, which is not accommodated by the horizontal strip theory.

Expression (5.5) is complicated to evaluate, so we present polynomial approximations with a relative error of less than 2%, for small, medium and large h:

$$I(h) = \begin{cases} \dfrac{28\zeta(3)}{\pi^3} h^2 - 0.3h^3 - 0.03h^4, & 0 < h < 1, \\ -0.64 + 1.36h + 0.025h^2, & 1 < h < 5, \\ -1.12 + \dfrac{\pi h}{2}, & 5 < h < 150. \end{cases} \tag{5.6}$$

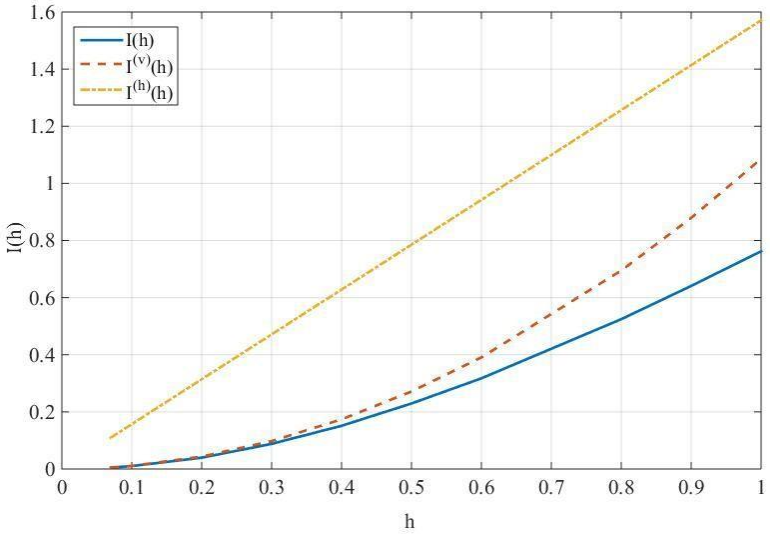

Figure 4. Total impulse exerted on a vertical plate as a function of the aspect ratio $h = H/L$ in the range [0, 1].

6. 3D water impact onto a vertical circular cylinder

The results of the previous sections, which were obtained from the pressure-impulse theory, can be applied to the 3D unsteady problem of water impact onto a vertical cylinder with constant and smooth horizontal cross sections. The configuration of the problem is the same as in figure 1 but with the plate replaced with a cylinder. A circular cylinder of radius R is considered here but the approach can be applied to other smooth cylindrical shapes as well. In this section the original dimensional variables are used.

The early stage of water impact on the circular cylinder of radius R is studied within both the von Karman and the Wagner [38] models of the water impact (figure 5). The models are valid during the initial stage, when the displacement of the wave front along the x-axis, Vt, is much smaller than the radius R, where V is the speed of the water front. We shall first analyze the Wagner model. The von Karman model is then a simplification of the Wagner model.

We assume that the horizontal dimension of the wetted part of the cylinder which is of order $O(\sqrt{VtR})$ during the early stage, is comparable with the water depth H. Hence $VtR = O(H^2)$. Then the condition $Vt \ll R$ implies that $H \ll R$. Therefore the 3D Wagner model can be used for vertical cylinders or panels of small curvature where the horizontal dimension of the contact region is of the same order as the water depth.

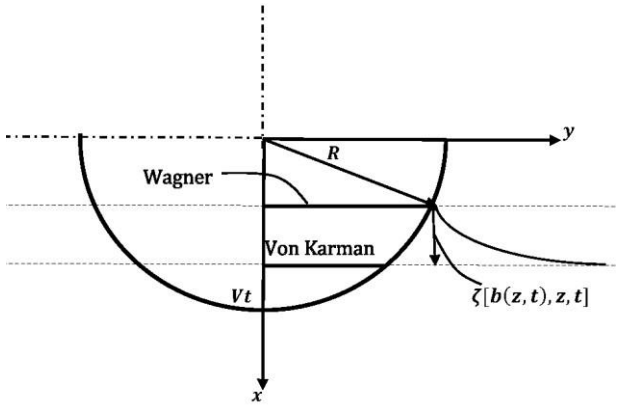

Figure 5. Plan view of the circular cylinder showing the von Karman and the Wagner approaches to the instantaneous positions of the wetted region.

Within the Wagner model of water impact, the boundary conditions are linearized and imposed on the initial positions of the liquid boundaries at the instant of impact, $t = 0$ [38]. The size of the wetted part of the cylinder, where the linearized body boundary condition, $\phi_x = V$, is imposed, is governed by the Wagner condition. This condition implies that the vertical boundary of the water front is continuous at contact lines, $y = \pm b(z,t)$ where $b(z,0) = 0$. Note that, in general, the unknown function $b(z,t)$ depends on the vertical coordinate z. That is, the contact region is bounded below by the bottom, $z = -H$, bounded above by the upper free-surface, $z = 0$, and by curvilinear boundaries $y = \pm b(z,t)$ at the right- and left-contact lines.

Let $x = \zeta(y, z, t)$ be the displacement of the wave front outside the contact region, where $|y| > b(z,t)$. Then the Wagner condition provides the equation for the unknown function $b(z,t)$,

$$\zeta[b(z),z]=\sqrt{R^2-b^2(z)}-R+Vt \tag{6.1}$$

The Wagner condition should be satisfied together with the Laplace equation for the velocity potential $\phi(x,y,z,t)$ in the flow region, the kinematic and dynamic boundary conditions on the free surface and the body boundary condition $\phi_x = V$ in the impact region, $x = 0$, $|y| < b(z,t)$, $-H < z < 0$. The displacement of the initially vertical free surface, $x = \zeta(y,z,t)$, is given by the linearized kinematic boundary condition, $\phi_x = \zeta_t$, where $x = 0, |y| > b(z,t)$. The Wagner condition can be readily satisfied in 2D [39] and axisymmetric [40] impact problems. In truly 3D problems of water impact this condition is difficult to satisfy [40]. Analytical solutions of the 3D impact problems are known only for elliptic contact regions [14, 17]. In the von Karman model, the displacement of the free surface, $\zeta(y,z,t)$, is not taken into account in the calculation of the size of the contact region. That is, the left hand-side in (6.1) is set zero which gives the width of the contact region independent of the vertical coordinate z within the von Karman model.

During the early stage, when $b \ll H$, we assume that the size of the contact region can be well approximated by the corresponding 2D solution (independent of z) far from the upper free-surface. This 2D solution suggests

$$b(z,t) \approx b_w(t) \tag{6.2}$$

where the function $b_w(t)$ satisfies the following equation [41]:

$$E\left[\frac{b_w(t)}{R}\right] = \frac{\pi}{2}\left(1 - \frac{Vt}{R}\right). \tag{6.3}$$

The function E in (6.3) denotes the complete elliptic integral of the second kind. The approximation (6.3) is not valid near the upper free-surface at $z = 0$. The dynamic boundary condition, $\phi = 0$, on the upper free surface, $z = 0$, implies that the horizontal components of the velocity ϕ_x and ϕ_y are zero there. They are also zero at the edge of the upper free surface, where $\phi = 0$, $x = 0$, $-\infty < y < \infty$. Then the kinematic condition, $\phi_x(0,y,z,t) = \zeta_t(y,z,t)$ on the edge $z = 0$ and $x = 0$, implies $\zeta_t(y,0,t) = 0$ and the Wagner condition (6.1) yields $\sqrt{R^2 - b^2(0,t)} - R + Vt = 0$. Hence,

$$b(0,t) = \sqrt{2Rt - (Vt)^2}. \tag{6.4}$$

which is the horizontal half-length of the contact region within the von Karman model of water impact.

We assume that at each time instant t the function $b(z,t)$ starts from the value (6.4) at $z = 0$ and increases monotonically with the distance from the upper free surface approaching $b_w(t)$ given by (6.3) as $z \to -H$, if the water is deep enough. We cannot prove this statement at this stage. To prove it, one needs to solve the 3D problem of water impact on a vertical cylinder, find the function $b(z,t)$ as part of the solution and compare it with the function $b_w(t)$ from (6.3).

The assumption $b(0,t) \le b(z,t) \le b_w(t)$, where $-H \le z \le 0$, allows us to estimate the hydrodynamic force $F(t)$ exerted on the circular cylinder. It is assumed that

$$F_0(t) \le F(t) \le F_w(t) \tag{6.5}$$

where $F_0(t)$ and $F_w(t)$ are the forces obtained for the contact regions $|y| < b(0,t)$ and $|y| < b_w(t)$, respectively, where $-H \le z \le 0$. Note that $b(0,t)$ and $b_w(t)$ (the von Karman and the Wagner dimensions of the contact region) are known functions of time from (6.3) and (6.4) such that $b(0,0) = 0$ and $b_w(0) = 0$.

It is convenient to introduce the non-dimensional variables

$$x = B(t)\hat{x},\ y = B(t)\hat{y},\ z = B(t)\hat{z},\ \phi = VB(t)\hat{\phi}(\hat{x},\hat{y},\hat{z},t), \tag{6.6}$$

where $B(t) = b(0,t)$ or $B(t) = b_w(t)$ and the wetted part of the cylinder is $|y| < B(t)$, $-H \le z \le 0$.

The potential $\hat{\phi}(\hat{x},\hat{y},\hat{z},t)$ satisfies the boundary-value problem (2.2)-(2.6) where $h = H/B(t)$. Note that the time t plays the role of a parameter in the linearized hydrodynamic problem with respect to the velocity potential $\phi(x,y,z,t)$. Therefore, the non-dimensional potential $\hat{\phi}(\hat{x},\hat{y},\hat{z},t)$ in the contact region, $\hat{x} = 0$, $|\hat{y}| < 1$, $-h(t) < \hat{z} < 0$, is given by (3.16). The hydrodynamic force $F_B(t)$ calculated within the linearized model with the width of the contact region being $2B(t)$ is given by

$$F_B(t) = -\rho \int_{-H}^{0} \int_{-B(t)}^{B(t)} \phi_t(0,y,z,t)\, dy\, dz = -\rho \frac{d}{dt} \int_{-H}^{0} \int_{-B(t)}^{B(t)} \phi(0,y,z,t)\, dy\, dz$$

$$= -\rho \frac{d}{dt} [VB^3(t) \int_{-h(t)}^{0} \int_{-1}^{1} \hat{\phi}(0,\hat{y},\hat{z},t)\, d\hat{y}\, d\hat{z}]. \tag{6.7}$$

In (6.7) we use the condition that the potential ϕ is zero along the lines $y = \pm B(t)$, $-H \le z \le 0$. The double integral in (6.7) is equal to $-I(h)$, where the total impulse, $I(h)$, introduced by (5.2) is given by (5.5). Therefore

$$F_B(t) = \rho V \frac{d}{dt}\{B^3(t)[H/B(t)]I(h)\} = \rho V B^2(t)B(t)[3I(h) - hI'(h)], \tag{6.8}$$

where dot denotes time derivative and $h = H/B(t)$. The total impulse $I(h)$ was investigated in Section 5 and $I'(h)$ is found numerically. During the early stage, $B(t) \ll H$, formula (5.3) implies $I(h) \sim \pi h/2$ as $h \to \infty$. Hence

$$F_B(t) \sim \rho V B \dot{B} \pi H \tag{6.9}$$

as $h \to \infty$, where $2B(t)H$ is the impact area at time t. The hydrodynamic force can be normalized as

$$\frac{F_B(t)}{F_{B,sc}(t)} \quad \frac{3I(h) - hI'(h)}{\pi h} = \tilde{F}_B(h), \tag{6.10}$$

where the force scale $F_{B,sc}(t)$ is given by the right-hand side of (6.9). Equation (6.10) shows that the non-dimensional force $\tilde{F}_B(h)$ depends on a single parameter h. Here $\tilde{F}_B(h) \to 1$ as $h \to \infty$ and $\tilde{F}_B(h) \approx 28\zeta(3)h/\pi^4$ as $h \to 0$, as follows from (5.4). The forces $\tilde{F}_B(h)$ calculated for $B = b_0(t)$ and $B = b_w(t)$ provide bounds for the hydrodynamic force $F_B(t)/F_{B,sc}(t)$ computed for the 3D contact region within the Wagner approach. The function $\tilde{F}_B(h)$ is depicted in figure 6 and clearly complies with the asymptotics $\tilde{F}_B(h) \to 1$ as $h \to \infty$ and $\tilde{F}_B(h) \sim 28\zeta(3)h/\pi^4 \approx 0.3455h$ as $h \to 0$.

The 2D approximation of the hydrodynamic force (6.9), normalized by $(1/2)\pi\rho V^2 HR$ reads

$$f_B = \frac{F_B(t)}{(1/2)\rho V^2 HR} = 2\frac{d(B/R)}{d\tau}(B/R), \tag{6.11}$$

where $\tau = Vt/R$ is the scaled time. Taking $B = b(0,t)$ for the von Karman model, we find

$$f_B = 2(1-\tau), \text{ for } B = b(0,t). \tag{6.12}$$

For the Wagner model with $B = b_w(t)$ we use (6.3) and, after some algebra, we obtain

$$f_B = \frac{\pi(B/R)^2}{K(B/R) - E(B/R)}, \text{ for } B = b_w(t) \tag{6.13}$$

where $K(B/R)$ denotes the complete elliptic integral of the first kind. Equations (6.12) and (6.13) provide the 2D von Karman and Wagner approximations, respectively, of the force exerted on a circular cylinder. The force (6.13) was derived by Korobkin [41, figure 4], with a different normalization. The 2D approximations (6.12) and (6.13) are compared with the 3D force (6.8). Using (6.8) and (6.10) it can be shown that the hydrodynamic force is

$$f_B = \frac{F_B(t)}{(1/2)\rho V^2 HR} = [2\frac{d(B/R)}{d\tau} - \varepsilon(B/R)]\tilde{F}_B\left(\frac{\varepsilon}{B/R}\right), \tag{6.14}$$

where $\varepsilon = H/R$ denotes the aspect ratio of the circular cylinder. The term in brackets is given by (6.12) and (6.13) for the von Karman and the Wagner models, respectively. Figure 7 compares the forces predicted by the 2D approximation and the present 3D method for $\varepsilon = 1$, using both models of wave impact. As implied by (6.12) the 2D force f_B from the von Karman model with $B = b(0,t)$ decreases linearly from 2 with increasing τ. It is interesting to observe that the 2D Wagner approach for $B = b_w(t)$ leads to a nearly linear decay of the force. In both cases the maximum non-dimensional force occurs at the first instant of impact and then decay, while the contact region widens. As expected, the Wagner approach leads to larger hydrodynamic loads than the von Karman approach due to the larger area of the contact region.

The results obtained using the present method, in particular (6.14), show a notable difference between the 2D and 3D forces for both models employed. However, the 2D approximations reproduce well the maximum loading that occurs at $\tau = 0$. The 3D forces are smaller and decay

much quicker with time than their 2D approximations. The forces from the 2D strip approach overestimates considerably the actual loading exerted on the circular cylinder.

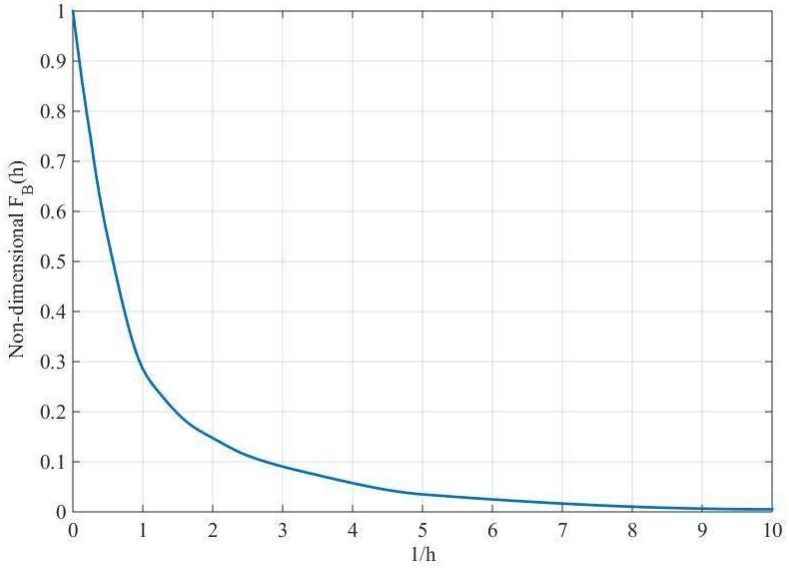

Figure 6. Non-dimensional hydrodynamic force (6.10) as a function of $1/h$.

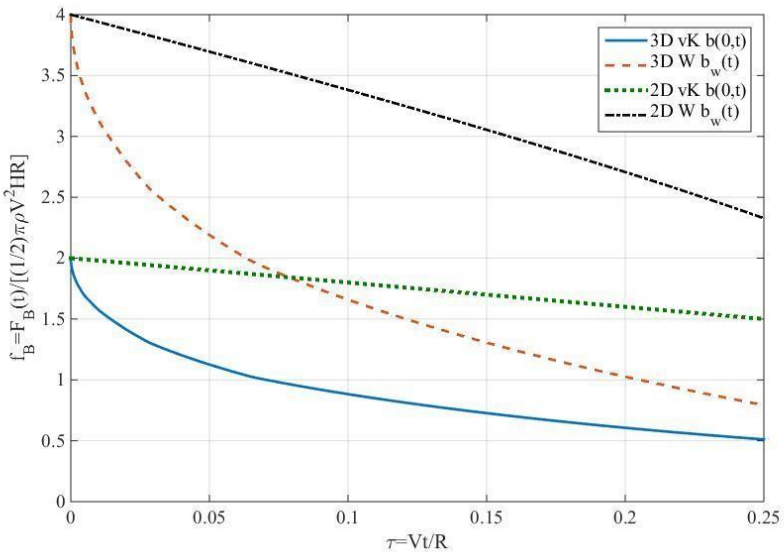

Figure 7. The non-dimensional hydrodynamic forces $f_B(\tau)$ by 2D von Karman model (6.12) and 2D Wagner model (6.13), and the 3D model (6.14) as functions of the non-dimensional time $\tau = Vt/R$ for $H/R = 1$.

7. Validation

The 3D theory of water impact developed in this paper can be applied to structures with either flat or convex surfaces. To validate this theory, the theoretical total impulse is compared with that for

the 3D wave impact onto a rectangular column with the wave front resembling the face of a steep wave, see [8]. The simulated case concerned a dam-break flow impact onto a rectangular column with square cross section 0.12×0.12m. The distance between the column and the dam was 0.5m. The water front arrived at the column about 0.25s after the flow starts. Cummins et al. [8] studied this problem numerically by a SPH method and compared the forces and the total impulse with experimental results. The total impulse on the column was evaluated by

$$I(t) = \int_0^t |F(\tau)| d\tau, \tag{7.1}$$

where $|F(\tau)|$ is the magnitude of the hydrodynamic load exerted on the column. Figure 5 in [8] shows a nearly vertical front face of the dam-break wave at the instant of impact, the height of which is estimated to be $H = 0.16$ m which leads to the aspect ratio $h \approx 2.6$ in our theory. It is difficult to extract the velocity of the wave front from both the numerical results and the experimental measurements presented in [8]. The velocity of the wave front is assumed equal to the critical velocity $V = \sqrt{gH} \approx 1.3$ m/s, where g is the gravitational acceleration. Using the scale of the total impulse, 0.28 Ns, and approximation (5.6) for the non-dimensional total impulse, $I(2.6) \approx 3.15$, the dimensional total impulse is 0.88 Ns, while figure 8 in Cummins et al. [8] estimates the total impulse, up to the instant of the maximum loading, to be about 0.9 Ns. This favorable agreement verifies the efficacy of the developed 3D impact theory of this paper.

8. Conclusions

The 3D hydrodynamic loads exerted on a rigid plate of finite dimensions by the impact of a rectangular liquid region have been studied within the pressure-impulse theory. The 3D distributions of pressure-impulse over the plate have been determined. The effect of the plate aspect ratio on the pressure-impulse distributions has been studied. Both the pressure-impulse and the total impulse (the time-integral of the hydrodynamic force), are strongly dependent on the 3D effects. The 2D approximations of the total impulse provided by the strip theory can be used with vertical strips if the water depth is one-tenth of the width of the plate, and with horizontal strips and a correction by an additive constant (of value about -1.12) if the water depth is three times larger than the width of the plate.

The developed 3D pressure-impulse theory has been extended to tackle the 3D unsteady problem of water impact onto a circular cylinder. Both the von Karman and the Wagner models of water

impact have been employed. The new model of 3D impact assumes straight vertical contact lines provided either by the von Karman or the Wagner 2D models. The pressure distribution in such contact regions is given by the 3D theory. This new 3D model provides bounds on the hydrodynamic force. Closed-form relations have been derived for both 2D and 3D approaches using both models of wave impact. It has been shown that the 3D hydrodynamic force exerted on the cylinder and normalized by the force provided by the 2D strip theory approximation, is a function of only the horizontal dimension of the contact region. Also, it has been shown that the 2D approach significantly overestimates the hydrodynamic load on the cylinder. This finding concerns both models of impact. Further, it was found that the maximum loading occurs at the start of impact, and is well reproduced by the 2D approaches. The 3D forces decay with time much faster than their 2D approximations.

The present study of 3D effects on impact loads is limited to simplified impact geometry. However, the methods and estimates obtained are expected to be valuable for practical applications such as tsunami bore, dry-bed surges, breaking and broken wave impact on coastal and offshore structures.

Ethics. This research poses no ethical considerations.

Data accessibility. This work does not have any experimental data.

Authors' contributions. MJC and AAK suggested the problem and conceived the mathematical formulation. All authors contributed to deriving the solutions. IKC developed the computer code and made the computations. All authors gave final approval for publication.

Competing interests. We have no competing interests.

Funding. This work was supported by the EU Marie Curie Intra-European Fellowships (FP7).

Acknowledgements. The authors are grateful to the EU Marie Curie Intra-European Fellowship project SAFEMILLS "Increasing Safety of Offshore Wind Turbines Operation: Study of the violent wave loads" under grant 622617.

References

1. Peregrine DH. 2003 Water-wave impact on walls. Ann. Rev. Fluid Mech., **35**, 23-43.
2. Ramsden JD. 1996 Forces on a vertical wall due to long waves, bores, and dry-bed surges. J Waterway, Port, Coastal and Ocean Eng., **122**, 134-141.

3. Robertson IN, Paczkowski K, Riggs HR. Mohamed A. 2011 Tsunami bore forces on walls. Proc. 30th Int. Conf. Ocean, Offsh. Arctic Eng., ASME, Rotterdam, The Netherlands, Paper No. OMAE2011-49487.
4. Ramsden JD. 1993 *Tsunamis: forces on a vertical wall caused by long waves, bores, and surges on a dry bed*, Doctoral Dissertation, California Institute of Technology.
5. Ramachandran K. 2015 Broken wave loads on a vertical wall: Large scale experimental investigations. Proc. 6th Int. Conf. Struct. Eng. Constr. Man., Kandy, Sri Lanka, 116-124.
6. Korobkin AA, Khabakhpasheva TI, Malenica S. 2016 Deformations of an elastic clamped plate in uniform flow and due to jet impact. Proc. 31st Int. Workshop Water Waves Float. Bod., Plymouth, MI, USA, 85-88.
7. Kleefsman KMT, Fekken G, Veldman AEP, Iwanowski B, Buchner B. 2005 A Volume-of-Fluid based simulation method for wave impact problems. J Comp. Phys., **206**, 363-393.
8. Cummins SJ, Silvester TB, Cleary PW. 2012 Three-dimensional wave impact on a rigid structure using smoothed particle hydrodynamics. Int. J Num. Methods Fluids, **68**, 1471-1496.
9. Cooker MJ, Peregrine DH. 1995 Pressure-impulse theory for liquid impact problems. J Fluid Mech., **297**, 193-214.
10. Korobkin AA. 2008 Wagner theory of steep wave impact. Proc. 23rd Int. Workshop Water Waves Float. Bod., Jeju, South Korea, 13-16.
11. Peregrine DH, Thais L. 1996 The effect of entrained air in violent water wave impacts. J Fluid Mech. **325**, 377-398.
12. Korobkin AA. 2006 Two-dimensional problem of the impact of a vertical wall on a layer of a partially aerated liquid. J Applied Mech. Tech. Phys., **47**, 643-653.
13. Iafrati A, Korobkin AA. 2006 Breaking wave impact onto vertical wall. Proc. 4th Int. Conf. Hydroelas. Mar. Tech., Wuxi, China, 139-148.
14. Scolan Y-M, Korobkin AA. 2001 Three-dimensional theory of water impact. Part 1. Inverse Wagner problem. J Fluid Mech., **440**, 293-326.
15. Korobkin AA, Scolan Y-M. 2006 Three-dimensional theory of water impact. Part 2. Linearized Wagner problem. J Fluid Mech., **549**, 343-373.
16. Meyerhoff MK. 1970 Added masses of thin rectangular plates calculated from potential theory. J Ship Res., **14**, 100-111.
17. Scolan Y-M. 2014 Hydrodynamic impact of an elliptic paraboloid on cylindrical waves. J Fluids Struc., **48**, 470-486.

18. Bullock GN, Obharai C, Peregrine DH, Bredmose H. 2007 Violent breaking wave impacts. Part 1: Results from large-scale regular wave tests on vertical and sloping walls. Coastal Eng., **54**, 602-617.
19. Chan E-S, Cheong H-F, Tan B-C. 1995 Laboratory study of plunging wave impacts on vertical cylinders. Coastal Eng., **25**, 87-107.
20. Mogridge GR, Jamieson WW. 1980 Wave impact pressures on composite breakwaters. Proc. 19th Int. Conf. Coastal Eng., **2**, 1829-1848.
21. Hunt B. 1982 Asymptotic solution for dam break problem. J Hydraul. Div. ASCE, **108**, 115-126.
22. Glaister P. 1991 Solutions of a two dimensional dam break problem. Int. J Eng. Sci., **29**, 1357-1362.
23. Stansby PK, Chegini A, Barnes TCD. 1998 The initial stages of dam-break flow. J Fluid Mech., **374**, 407-424.
24. Brufau P., Garcia-Navarro P. 2000 Two dimensional dam break flow simulation. Int. J Numer. Methods Fluids Res., **33**, 35-57.
25. Zoppou C, Roberts S. 2000 Numerical simulation of the two-dimensional unsteady dam break. App. Math. Fluids Res., **24**, 457-475.
26. Zoppou C, Roberts S. 2003 Explicit schemes for dam-break simulations. J Hydraul. Eng., **129**, 11-34.
27. Korobkin AA, Yilmaz O. 2009 The initial stage of dam-break flow. J Eng. Math., **63**, 293-308.
28. Abdolmaleki K, Thiagarajan KP, Morris-Thomas MT. 2004 Simulation of the dam-break problem and impact flows using a Navier-Stokes solver. Proc. 15th Australian Fluid Mech. Conf., The University of Sydney, Sydney, Australia.
29. Aureli F, Dazzi S, Maranzoni A, Mignosa P, Vacondio R. 2015 Experimantal and numerical evaluation of the force due to the impact of a dam-break wave on a structure. Advances in Water Resources, **76**, 29-42.
30. Yang C, Lin B, Jiang C, Liu Y. 2010 Predicting near-field dam-break flow and impact force using a 3D model. J Hydraulic Res, **48**, 784-792.
31. Sneddon IN. 1966 *Mixed boundary value problems in potential theory*, Amsterdam: North Holland Publishing Company.
32. King AC, Needham DJ. 1994 Initial development of a jet caused by fluid, body and free-surface interaction. Part 1. A uniformly accelerating plate. J Fluid Mech., **268**, 89-101.
33. Egorov IT. 1956 Impact on a compressible fluid. NACA TM 1413 (Translation of "Udar o szhimaemuiu zhidkost"). Prikladnaia Matematika i Mekhanika, **20**, 67-72.

34. Abramowitz M, Stegun IA. 1970 *Handbook of mathematical functions*. New York, NY: Dover.

35. Gradshteyn IS, Ryzhik IM. 2007 *Table of integrals, series and products (seventh edition)*. London: Elsevier Academic Press.

36. Bagnold RA. 1939 Interim report on wave pressure research. J Inst. Civil Engrs., **12**, 201-226.

37. Richert G. 1968 Experimental investigation of shock pressures against breakwaters. Proc. 11th Conf. Coastal Eng, ASCE, 945-973.

38. Wagner H. 1932 Über Stross- und Gleitvorgänge an der Oberfläche von Flüssigkeiten. Z. Angew Math. Mech., **12**, 193-215.

39. Korobkin AA. 1985 Initial asymptotics of solution of three dimensional problem on a blunt body penetration into ideal liquid. Dokl. Akad. Nauk SSSR **283**, 838-842.

40. Gazzola T, Korobkin AA, Malenica S, Scolan Y-M. 2005. Three-dimensional Wagner problem using variational inequalities. In Proc. 20th Int. Workshop Water Waves Float. Bod., Spritzbergen, Norway, Paper No 17.

41. Korobkin AA. 2004 Analytical models of water impact. European J Applied Math., **15**, 821-838.

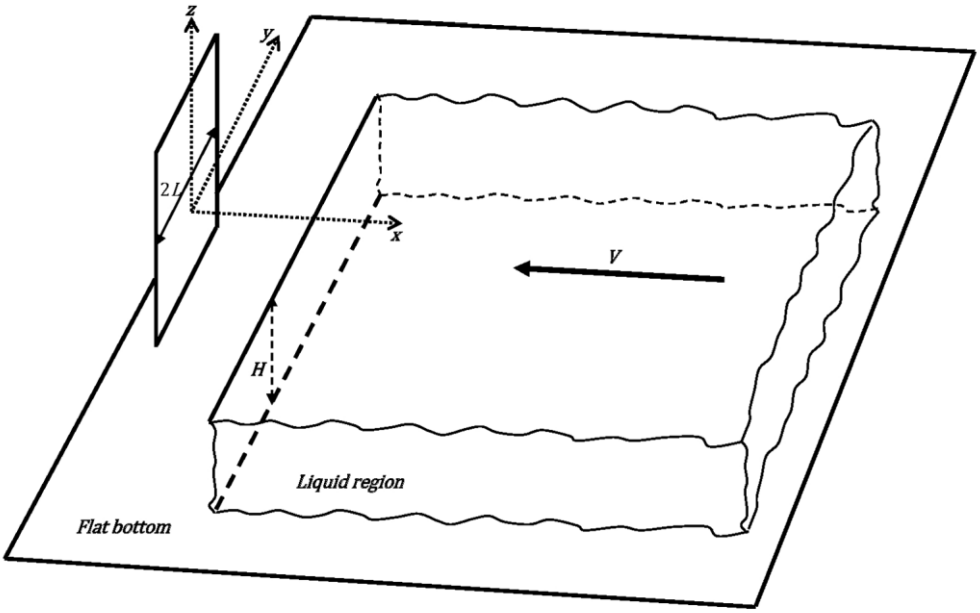

Figure 1. Configuration of the water impact problem with a vertical plate.
422x287mm (96 x 96 DPI)

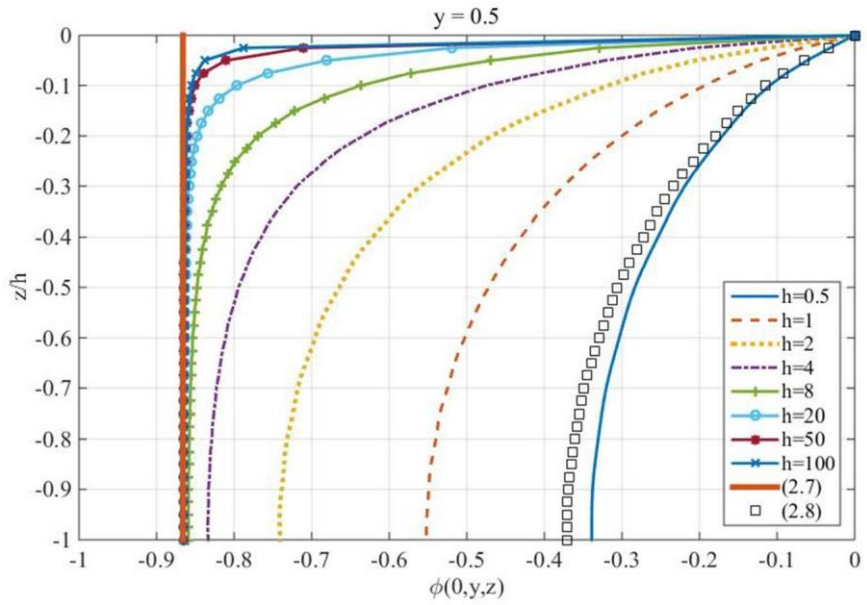

Figure 2. Vertical variation of the velocity potential (3.16) at x=0,y=0.5 for increasing aspect ratio h=H/L. The thick solid line depicts the 2D solution (2.7) which is approached by the 3D solution for h≫1. The square symbols '□' depict the 2D solution (2.8) with h=0.5.

318x216mm (72 x 72 DPI)

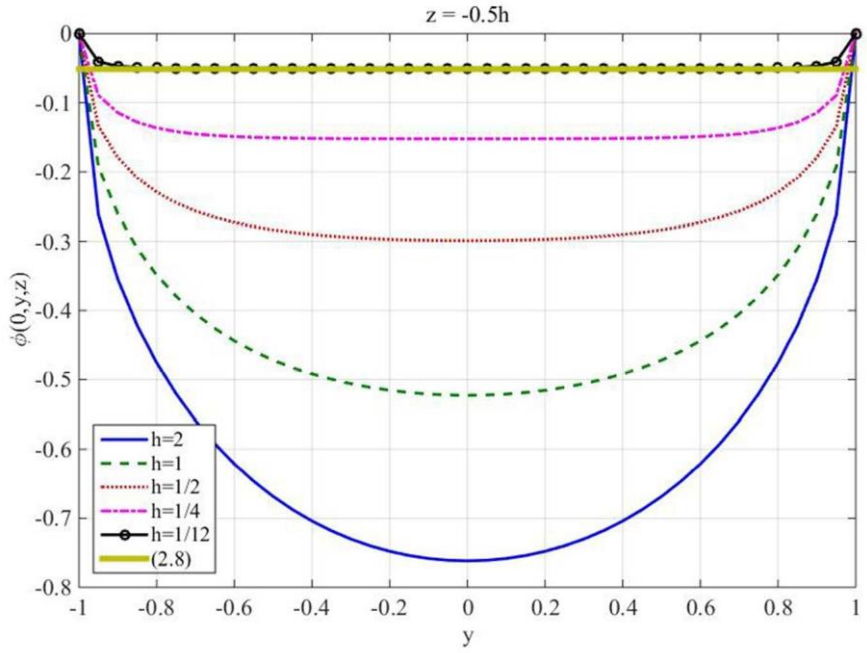

Figure 3. The velocity potential (3.16) at z/h=-0.5 for decreasing height to length ratio h=H/L. The thick solid line corresponds to the 2D approximation (2.8), which is valid for small h.
318x216mm (72 x 72 DPI)

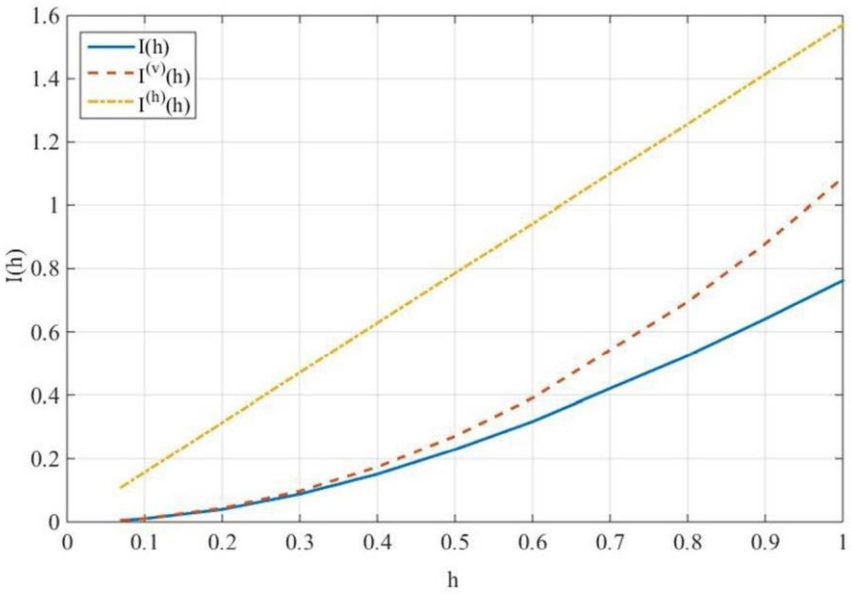

Figure 4. Total impulse exerted on a vertical plate as a function of the aspect ratio h=H/L in the range [0, 1].

318x216mm (72 x 72 DPI)

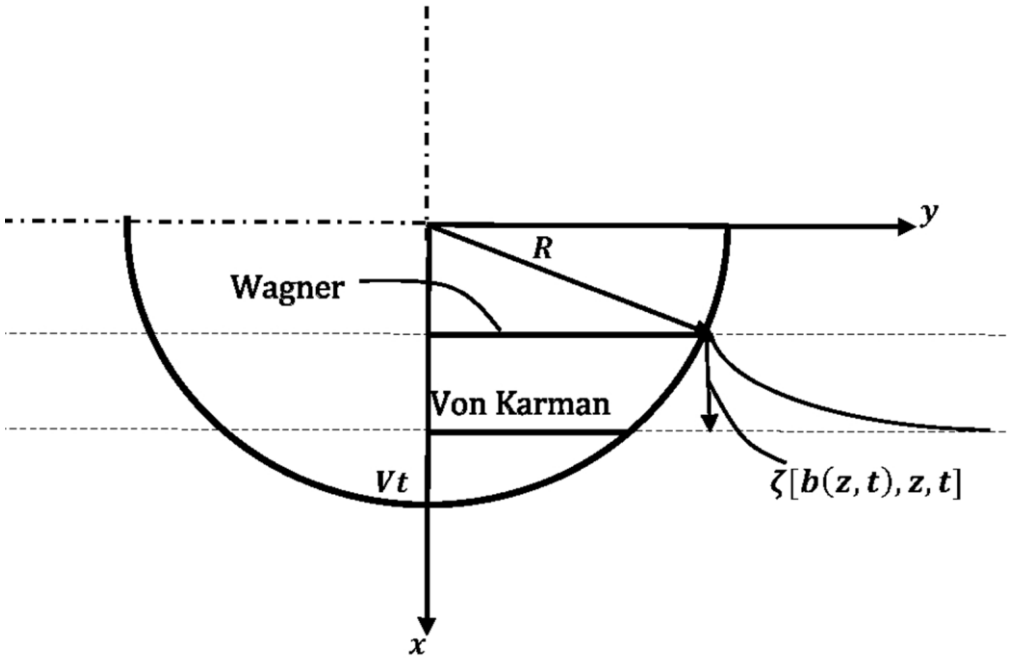

Figure 5. Plan view of the circular cylinder showing the von Karman and the Wagner approaches to the instantaneous positions of the wetted region.
255x170mm (96 x 96 DPI)

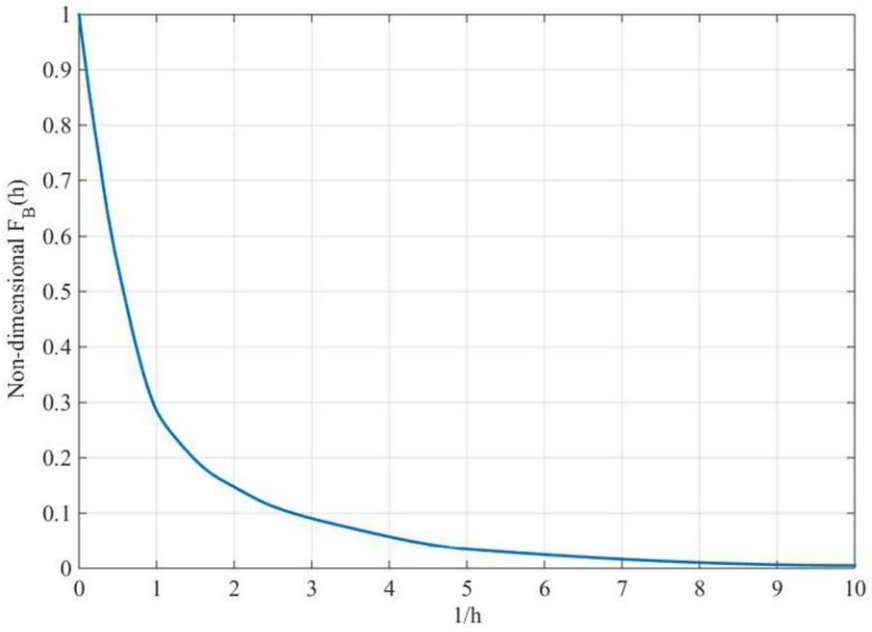

Figure 6. Non-dimensional hydrodynamic force (6.10) as a function of 1/h.
318x216mm (72 x 72 DPI)

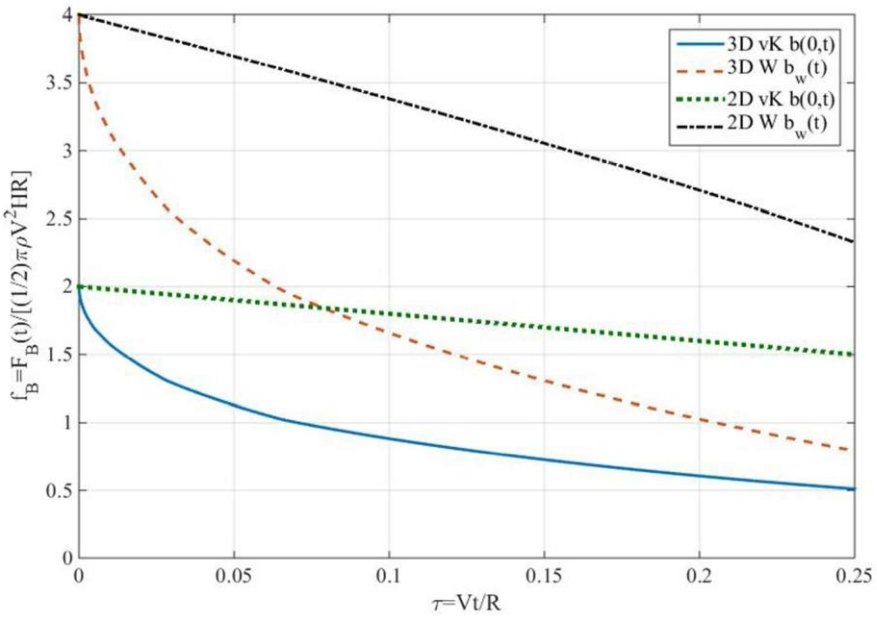

Figure 7. The non-dimensional hydrodynamic forces f_B (τ) by 2D von Karman model (6.12) and 2D Wagner model (6.13), and the 3D model (6.14) as functions of the non-dimensional time τ=Vt/R for H/R=1.
318x216mm (72 x 72 DPI)

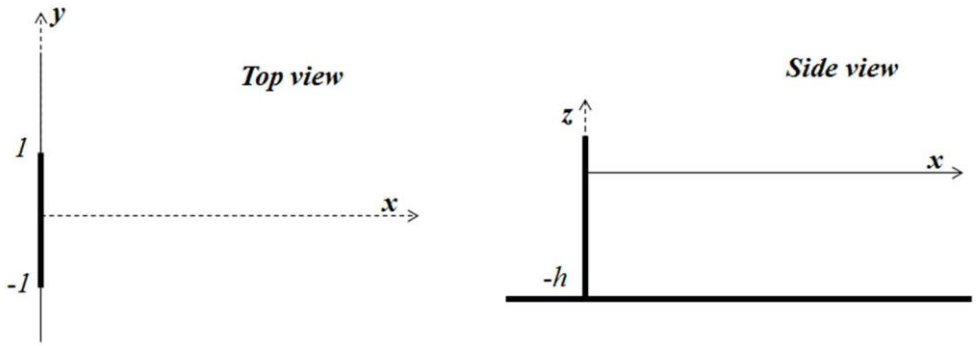

Figure A.1. Top and side views of the problem at the instant of impact; dimensionless variables.
221x100mm (96 x 96 DPI)

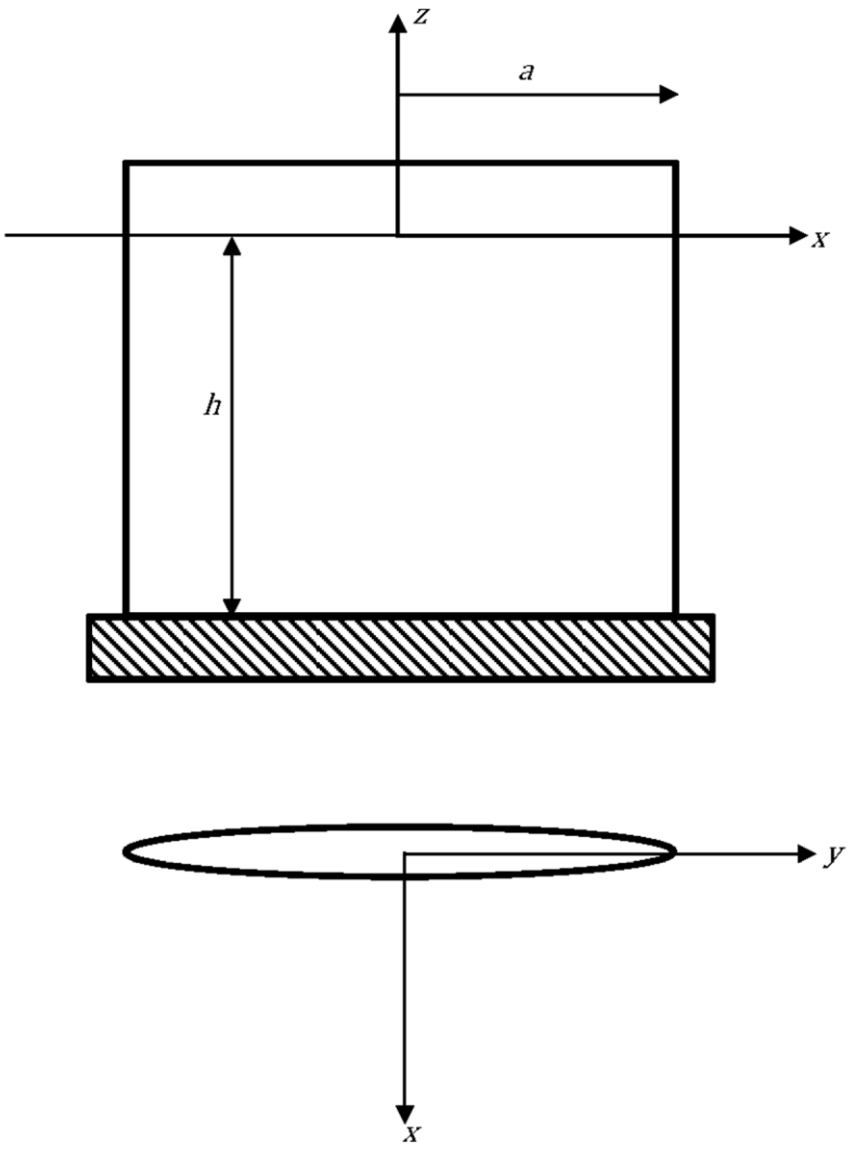

Figure A.2. Coordinates for the plate of elliptical cross section.
232x305mm (96 x 96 DPI)

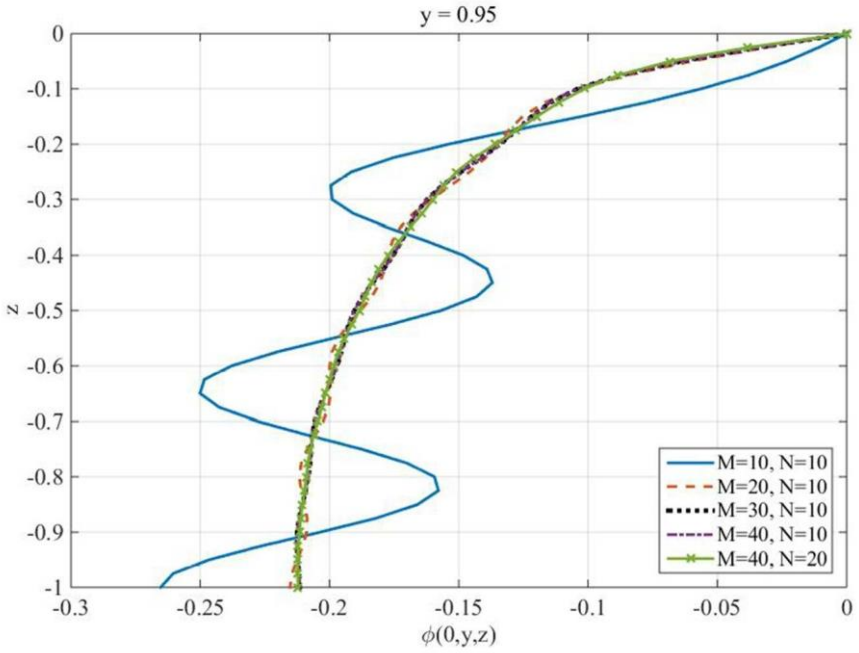

Figure A.3. Convergence study for the velocity potential (3.16) on the plate (x=0) close to its edge (y=0.95) for h=1. Here z varies on the plate from -1 (bottom) to 0 (upper free-surface). The truncation of the order of the Mathieu functions is M and N is the truncation of the vertical eigenfunctions with values shown in the caption legend.
318x216mm (72 x 72 DPI)

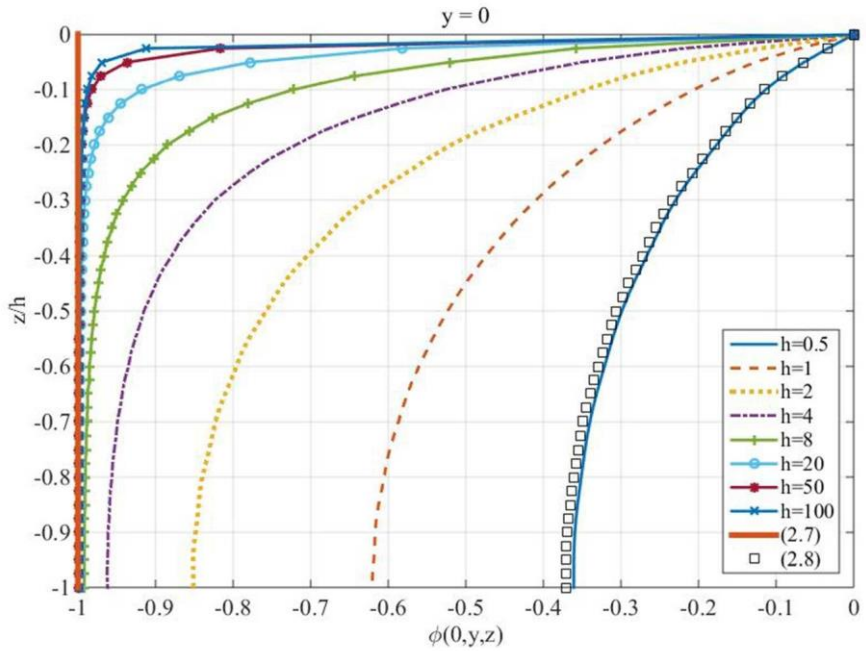

Figure A.4. Vertical variation of the velocity potential (3.16) at x=0,y=0 for increasing aspect ratio h=H/L. The thick solid line depicts the 2D solution (2.7) which is valid for h≫1. The square symbols '□' depict the 2D solution (2.8) with h=0.5.

318x216mm (72 x 72 DPI)

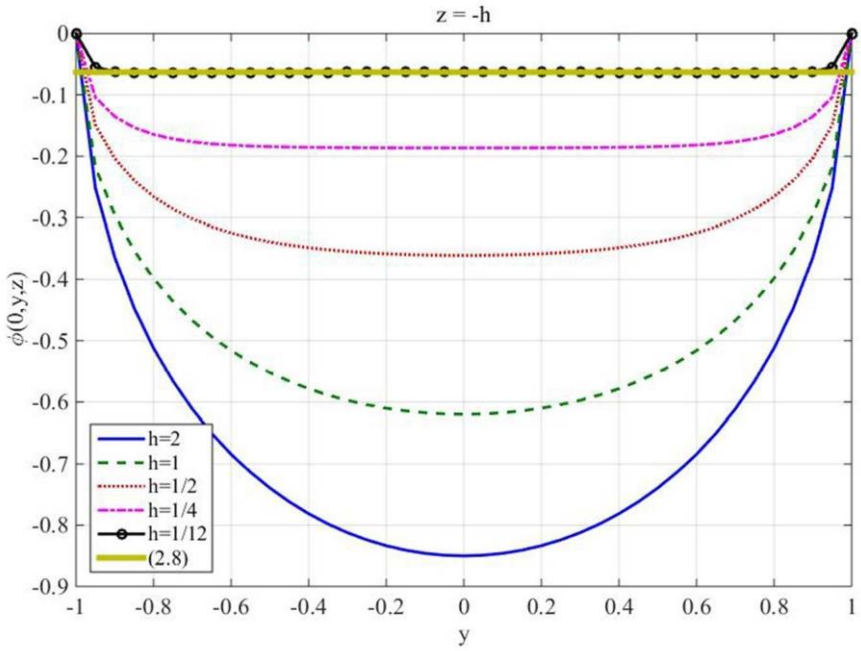

Figure A.5. The velocity potential (3.16) at z/h=-1 for decreasing height to length ratio h=H/L. Thethick solid line corresponds to the 2D approximation (2.8), which is valid for small h.

318x216mm (72 x 72 DPI)

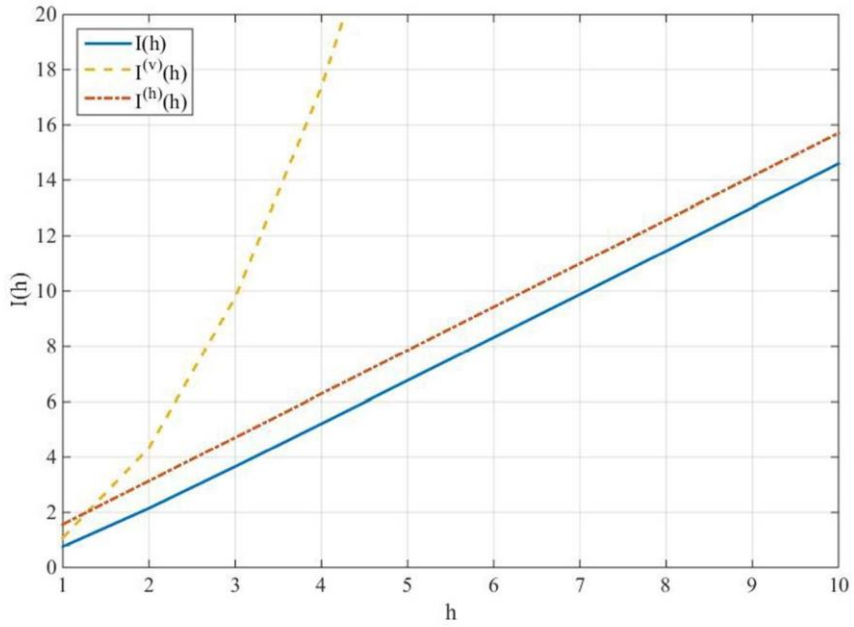

Figure A.6. Total impulse exerted on a vertical plate as a function of the aspect ratio h=H/L in the range [1, 10].

318x216mm (72 x 72 DPI)